Reservoir Imaging with Surface Waves

Yanhua O. Yuan

Princeton University

Ebru Bozdağ

Université de Nice

Frederik J. Simons

Princeton University

PART I

Parameterization of Global Models

Spherical harmonics, spherical harmonic splines, spherical wavelets

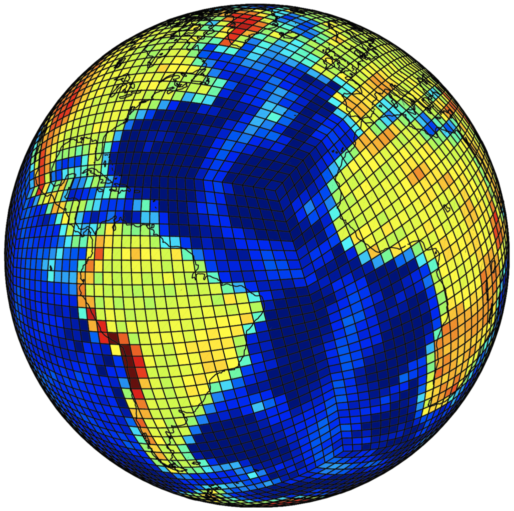

Part II

Mixed-norm Inversions at the Global Scale

Finite-frequency measurements, spatial wavelets, sparsity-seeking algorithms

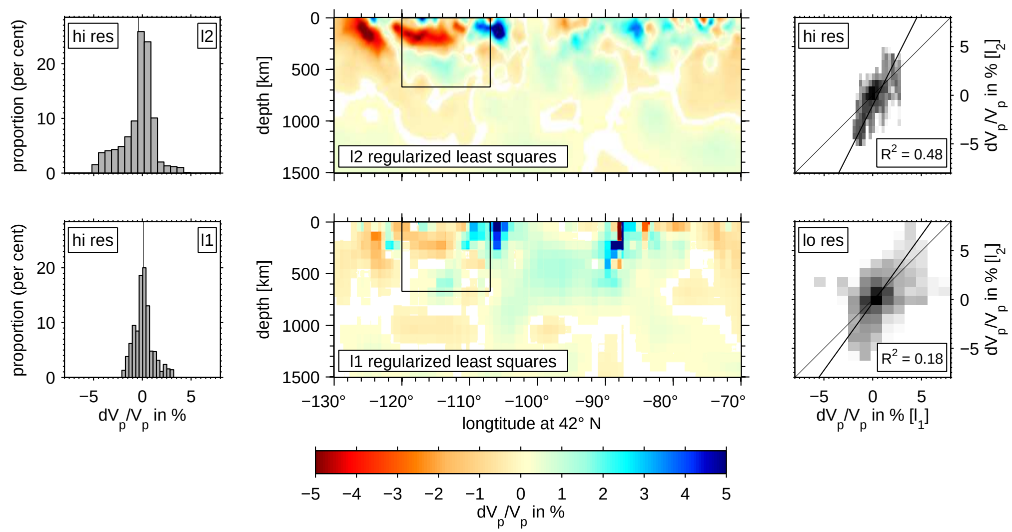

Part III

Multiscale Inversions of Exploration Models

Waveform differences, time-domain wavelets, spectral-element adjoint algorithms

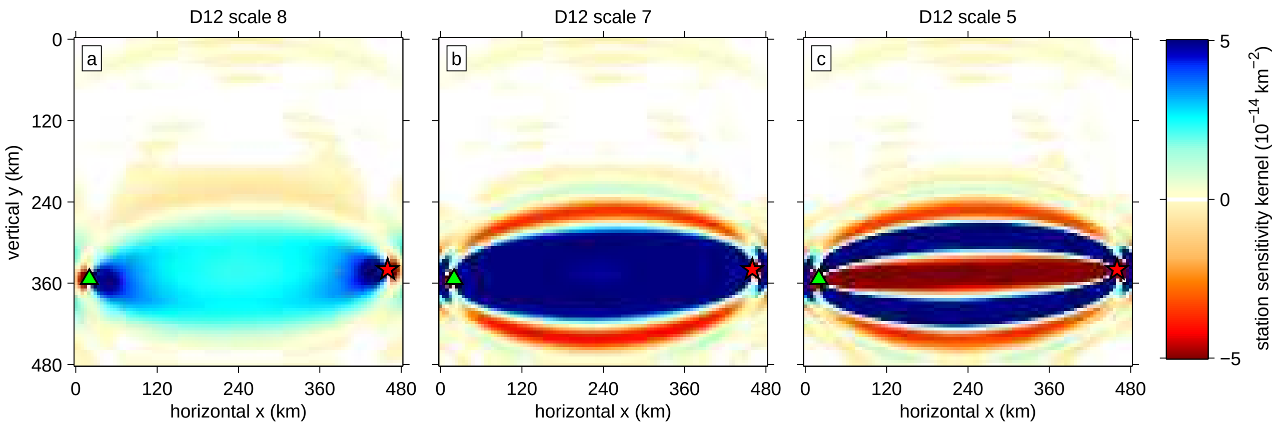

Waveform *difference*

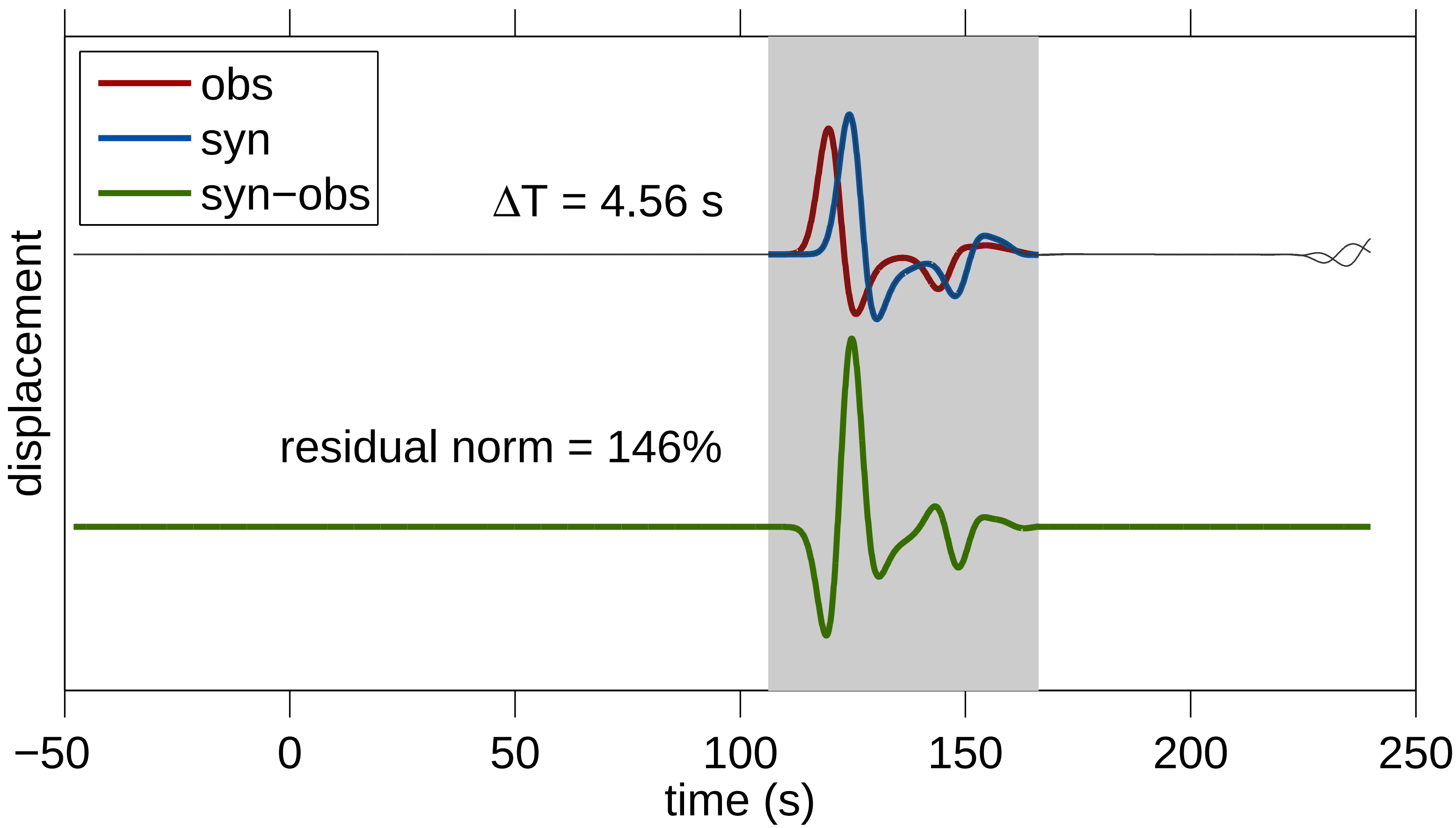

Yuan & Simons, *Geophysics* (2014)

Multiscale adjoint waveform-*difference* tomography

1. Misfit function for model $\mathbf{m}$, data $\mathbf{d}$, synthetic $\mathbf{s}$, location $\mathbf{x}$, time t:
   $\chi(\mathbf{m}) = \frac{1}{2} \sum_{s,r} \int_0^T ||\mathbf{s}(\mathbf{x}_r, \mathbf{x}_s, t; \mathbf{m}) - \mathbf{d}(\mathbf{x}_r, \mathbf{x}_s, t)||^2 \, dt$

Multiscale adjoint waveform-*difference* tomography

1. Misfit function for model $\mathbf{m}$, data $\mathbf{d}$, synthetic $\mathbf{s}$, location $\mathbf{x}$, time t:
   $\chi(\mathbf{m}) = \frac{1}{2}\sum_{s,r}\int_0^T ||\mathbf{s}(\mathbf{x}_r,\mathbf{x}_s,t;\mathbf{m}) - \mathbf{d}(\mathbf{x}_r,\mathbf{x}_s,t)||^2\,dt$
2. Fréchet derivative of $\chi(\mathbf{m})$ over all sources s, receivers r:
   $\delta\chi(\mathbf{m}) = \sum_{s,r}\int_0^T [\mathbf{s}(\mathbf{x}_r,\mathbf{x}_s,t;\mathbf{m}) - \mathbf{d}(\mathbf{x}_r,\mathbf{x}_s,t)]\cdot\delta\mathbf{s}(\mathbf{m})\,dt$

Multiscale adjoint waveform-*difference* tomography

1. Misfit function for model $\mathbf{m}$, data $\mathbf{d}$, synthetic $\mathbf{s}$, location $\mathbf{x}$, time t:
   $$\chi(\mathbf{m}) = \frac{1}{2}\sum_{s,r}\int_0^T ||\mathbf{s}(\mathbf{x}_r, \mathbf{x}_s, t; \mathbf{m}) - \mathbf{d}(\mathbf{x}_r, \mathbf{x}_s, t)||^2 \, dt$$
2. Fréchet derivative of $\chi(\mathbf{m})$ over all sources s, receivers r:
   $$\delta\chi(\mathbf{m}) = \sum_{s,r}\int_0^T [\mathbf{s}(\mathbf{x}_r, \mathbf{x}_s, t; \mathbf{m}) - \mathbf{d}(\mathbf{x}_r, \mathbf{x}_s, t)] \cdot \delta\mathbf{s}(\mathbf{m}) \, dt$$
3. Linearized expression under the Born approximation:
   $$\delta\chi = \int_V [K_\rho(\mathbf{x})\,\delta\rho(\mathbf{x}) + \mathbf{K}_{\mathbf{c}}(\mathbf{x}) :: \delta\mathbf{c}(\mathbf{x})]\, d^3\mathbf{x}$$

Multiscale adjoint waveform-*difference* tomography

1. Misfit function for model $\mathbf{m}$, data $\mathbf{d}$, synthetic $\mathbf{s}$, location $\mathbf{x}$, time t:

   $$\chi(\mathbf{m}) = \tfrac{1}{2} \sum_{s,r} \int_0^T ||\mathbf{s}(\mathbf{x}_r, \mathbf{x}_s, t; \mathbf{m}) - \mathbf{d}(\mathbf{x}_r, \mathbf{x}_s, t)||^2 \, dt$$

2. Fréchet derivative of $\chi(\mathbf{m})$ over all sources s, receivers r:

   $$\delta\chi(\mathbf{m}) = \sum_{s,r} \int_0^T [\mathbf{s}(\mathbf{x}_r, \mathbf{x}_s, t; \mathbf{m}) - \mathbf{d}(\mathbf{x}_r, \mathbf{x}_s, t)] \cdot \delta\mathbf{s}(\mathbf{m}) \, dt$$

3. Linearized expression under the Born approximation:

   $$\delta\chi = \int_V [K_\rho(\mathbf{x}) \, \delta\rho(\mathbf{x}) + \mathbf{K}_{\mathbf{c}}(\mathbf{x}) :: \delta\mathbf{c}(\mathbf{x})] \, d^3\mathbf{x}$$

4. Misfit kernel

   $$\mathbf{K}_{\mathbf{c}}(\mathbf{x}) = -\sum_{s,r} \int_0^T [\boldsymbol{\nabla}\mathbf{s}^\dagger(\mathbf{x}_r, \mathbf{x}, T-t)][\boldsymbol{\nabla}\mathbf{s}(\mathbf{x}, \mathbf{x}_s, t)] \, dt$$

Multiscale adjoint waveform-*difference* tomography

1. Misfit function for model $\mathbf{m}$, data $\mathbf{d}$, synthetic $\mathbf{s}$, location $\mathbf{x}$, time t:

   $$\chi(\mathbf{m}) = \frac{1}{2}\sum_{s,r}\int_0^T ||\mathbf{s}(\mathbf{x}_r, \mathbf{x}_s, t; \mathbf{m}) - \mathbf{d}(\mathbf{x}_r, \mathbf{x}_s, t)||^2 \, dt$$

2. Fréchet derivative of $\chi(\mathbf{m})$ over all sources s, receivers r:

   $$\delta\chi(\mathbf{m}) = \sum_{s,r}\int_0^T [\mathbf{s}(\mathbf{x}_r, \mathbf{x}_s, t; \mathbf{m}) - \mathbf{d}(\mathbf{x}_r, \mathbf{x}_s, t)] \cdot \delta\mathbf{s}(\mathbf{m}) \, dt$$

3. Linearized expression under the Born approximation:

   $$\delta\chi = \int_V [K_\rho(\mathbf{x})\,\delta\rho(\mathbf{x}) + \mathbf{K_c}(\mathbf{x}) :: \delta\mathbf{c}(\mathbf{x})] \, d^3\mathbf{x}$$

4. Misfit kernel

   $$\mathbf{K_c}(\mathbf{x}) = -\sum_{s,r}\int_0^T [\boldsymbol{\nabla}\mathbf{s}^\dagger(\mathbf{x}_r, \mathbf{x}, T - t)][\boldsymbol{\nabla}\mathbf{s}(\mathbf{x}, \mathbf{x}_s, t)] \, dt$$

5. The **adjoint** field $\mathrm{s}^\dagger$, calculated using the SPECFEM forward solver.

Multiscale adjoint waveform-*difference* tomography

1. Misfit function for model $\mathbf{m}$, data $\mathbf{d}$, synthetic $\mathbf{s}$, location $\mathbf{x}$, time t:

$$\chi(\mathbf{m}) = \frac{1}{2}\sum_{s,r}\int_0^T ||\mathbf{s}(\mathbf{x}_r,\mathbf{x}_s,t;\mathbf{m}) - \mathbf{d}(\mathbf{x}_r,\mathbf{x}_s,t)||^2\, dt$$

2. Fréchet derivative of $\chi(\mathbf{m})$ over all sources s, receivers r:

$$\delta\chi(\mathbf{m}) = \sum_{s,r}\int_0^T [\mathbf{s}(\mathbf{x}_r,\mathbf{x}_s,t;\mathbf{m}) - \mathbf{d}(\mathbf{x}_r,\mathbf{x}_s,t)]\cdot\delta\mathbf{s}(\mathbf{m})\, dt$$

3. Linearized expression under the Born approximation:

$$\delta\chi = \int_V [K_\rho(\mathbf{x})\,\delta\rho(\mathbf{x}) + \mathbf{K}_\mathbf{c}(\mathbf{x}) :: \delta\mathbf{c}(\mathbf{x})]\, d^3\mathbf{x}$$

4. Misfit kernel

$$\mathbf{K}_\mathbf{c}(\mathbf{x}) = -\sum_{s,r}\int_0^T [\boldsymbol{\nabla}\mathbf{s}^\dagger(\mathbf{x}_r,\mathbf{x},T-t)][\boldsymbol{\nabla}\mathbf{s}(\mathbf{x},\mathbf{x}_s,t)]\, dt$$

5. The **adjoint** field $\mathrm{s}^\dagger$, calculated using the SPECFEM forward solver.

6. Iterative inversions of this scheme need *some sort* of regularization to temper the non-linearity, stabilize the inversion, and speed up the convergence.

   The traditional way is to progressively **frequency-filter** the seismograms.

Multiscale adjoint waveform-*difference* tomography

1. Misfit function for model $\mathbf{m}$, data $\mathbf{d}$, synthetic $\mathbf{s}$, location $\mathbf{x}$, time t:
$$\chi(\mathbf{m}) = \frac{1}{2}\sum_{s,r}\int_0^T ||\mathbf{s}(\mathbf{x}_r,\mathbf{x}_s,t;\mathbf{m}) - \mathbf{d}(\mathbf{x}_r,\mathbf{x}_s,t)||^2\,dt$$
2. Fréchet derivative of $\chi(\mathbf{m})$ over all sources s, receivers r:
$$\delta\chi(\mathbf{m}) = \sum_{s,r}\int_0^T [\mathbf{s}(\mathbf{x}_r,\mathbf{x}_s,t;\mathbf{m}) - \mathbf{d}(\mathbf{x}_r,\mathbf{x}_s,t)]\cdot\delta\mathbf{s}(\mathbf{m})\,dt$$
3. Linearized expression under the Born approximation:
$$\delta\chi = \int_V [K_\rho(\mathbf{x})\,\delta\rho(\mathbf{x}) + \mathbf{K}_\mathbf{c}(\mathbf{x}) :: \delta\mathbf{c}(\mathbf{x})]\,d^3\mathbf{x}$$
4. Misfit kernel
$$\mathbf{K}_\mathbf{c}(\mathbf{x}) = -\sum_{s,r}\int_0^T [\boldsymbol{\nabla}\mathbf{s}^\dagger(\mathbf{x}_r,\mathbf{x},T-t)][\boldsymbol{\nabla}\mathbf{s}(\mathbf{x},\mathbf{x}_s,t)]\,dt$$
5. The **adjoint** field $\mathbf{s}^\dagger$, calculated using the SPECFEM forward solver.
6. Our innovation is to supply constructively approximated data, synthetics, and measurements, using **wavelets** up to scale j, within which we iterate:
$$\chi_j(\mathbf{m}) = \frac{1}{2}\sum_{s,r}\int_0^T ||\mathbf{s}_j(\mathbf{x}_r,\mathbf{x}_s,t;\mathbf{m}) - \mathbf{d}_j(\mathbf{x}_r,\mathbf{x}_s,t)||^2\,dt$$

Time domain, 1D wavelets

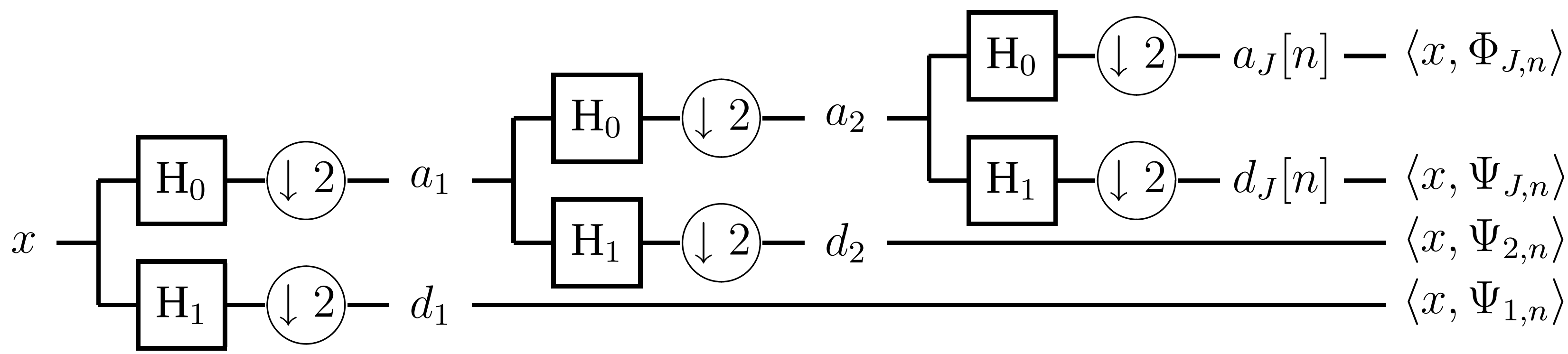

Time domain, 1D wavelets

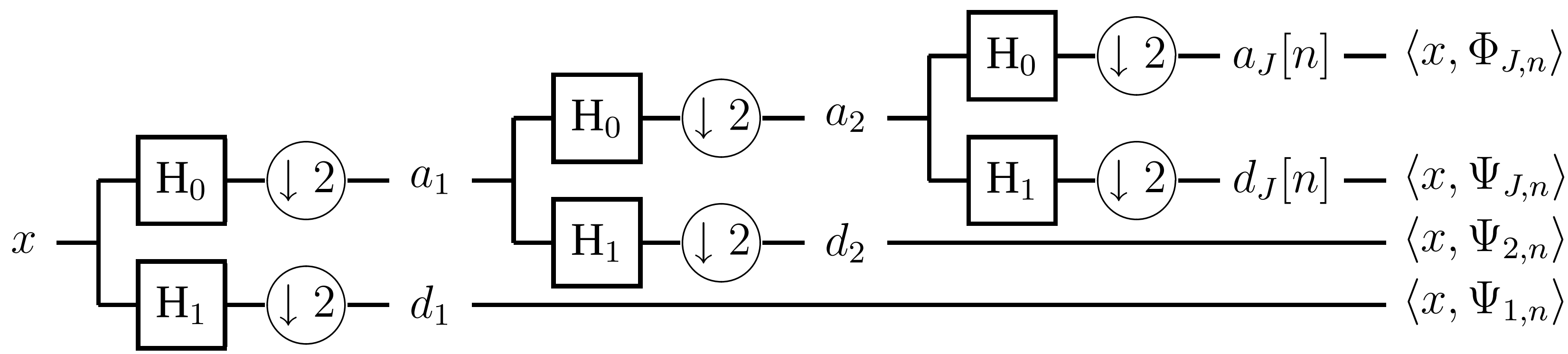

Partial reconstruction = **projection** of seismogram onto **subspace** of scale j:

$$x_j[n] = \sum_n a_{J,n} \phi_{J,n} + \sum_{j'=j+1}^{J} \sum_n d_{j',n} \psi_{j',n}. \tag{1}$$

A realistic synthetic model

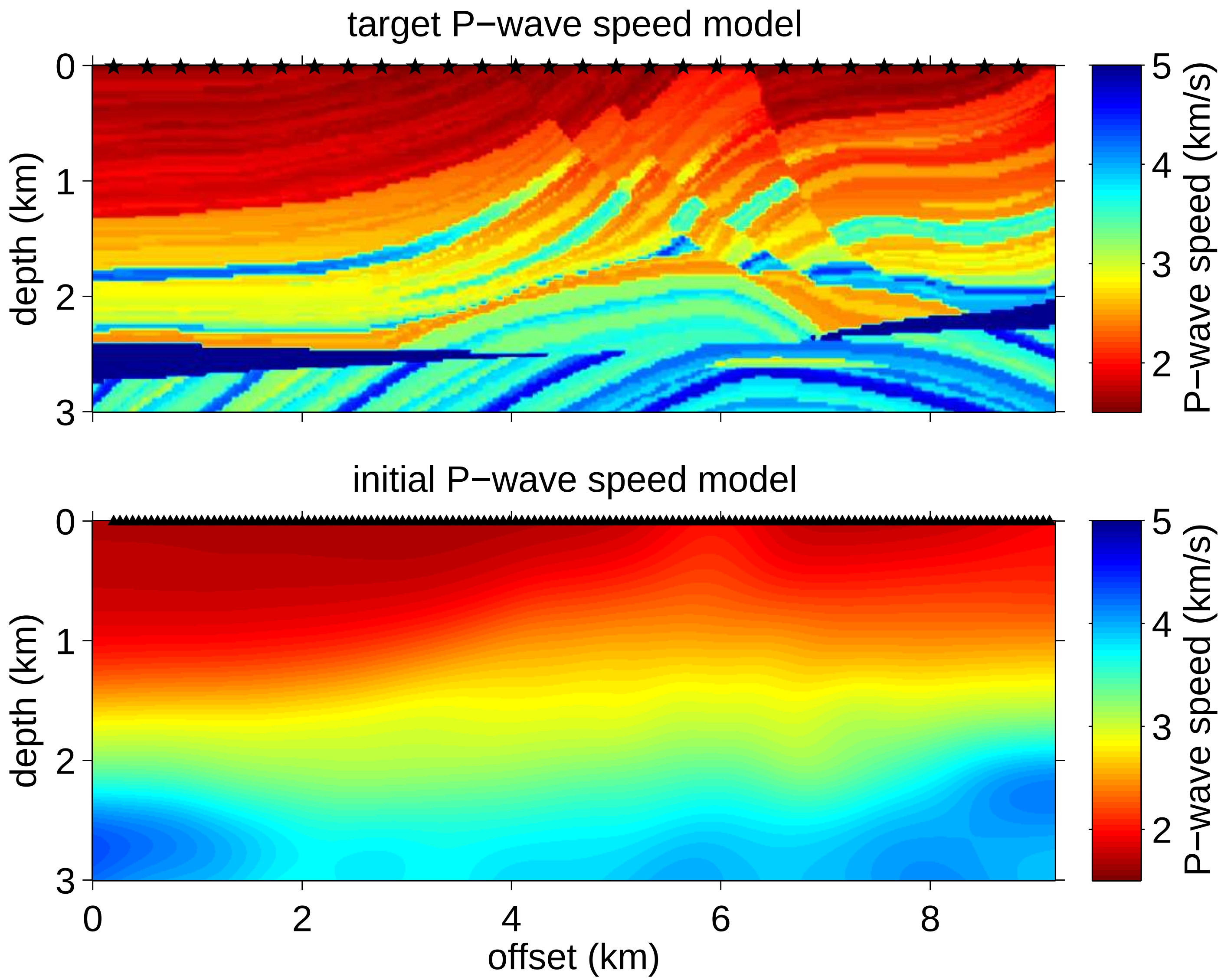

Yuan & Simons, *Geophysics* (2014)

Elastic data, with and without surface waves

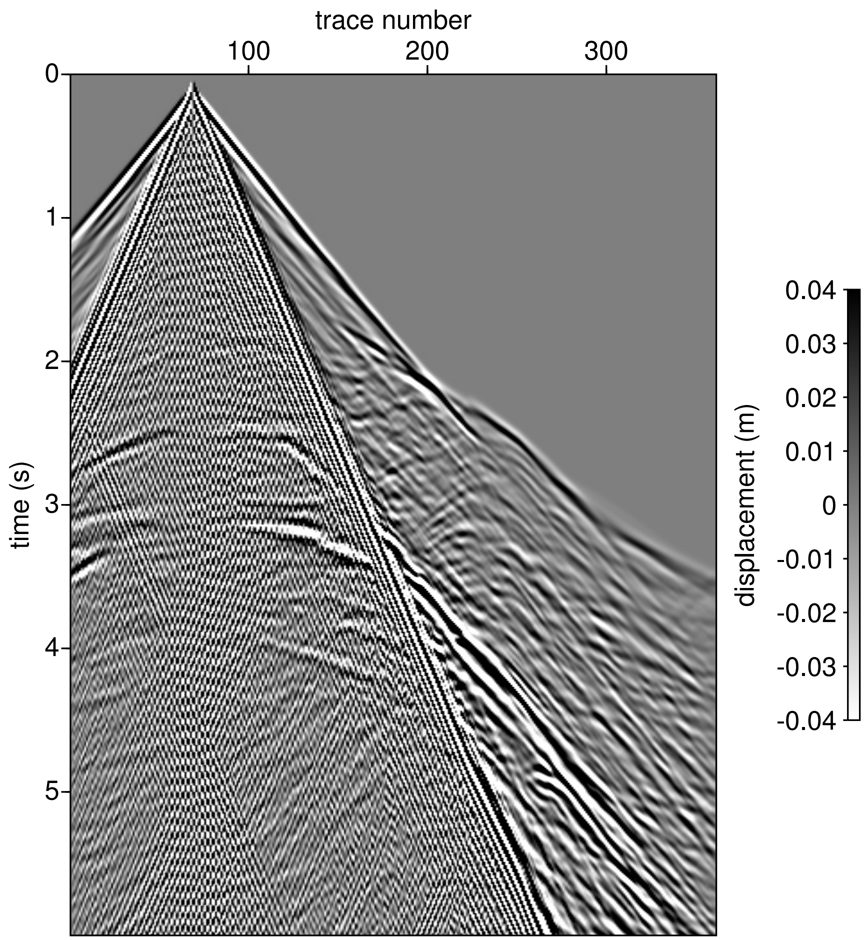

original data (shot 20, X-comp)

Elastic data, with and without surface waves

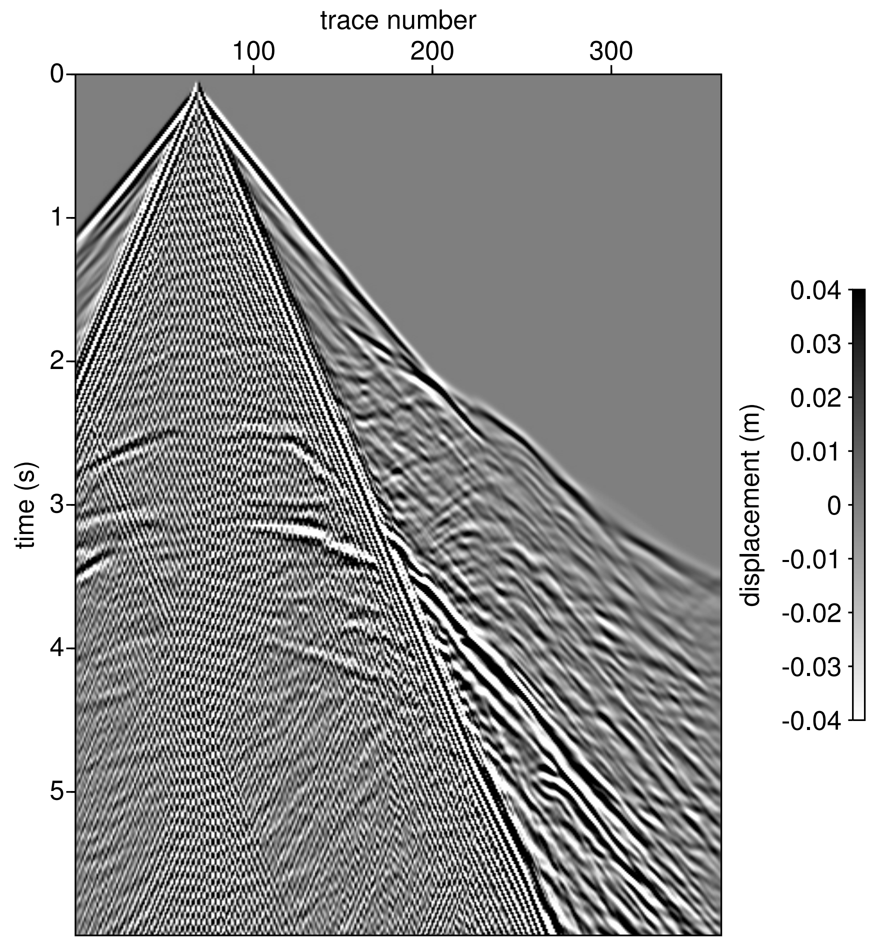

original data (shot 20, X-comp)

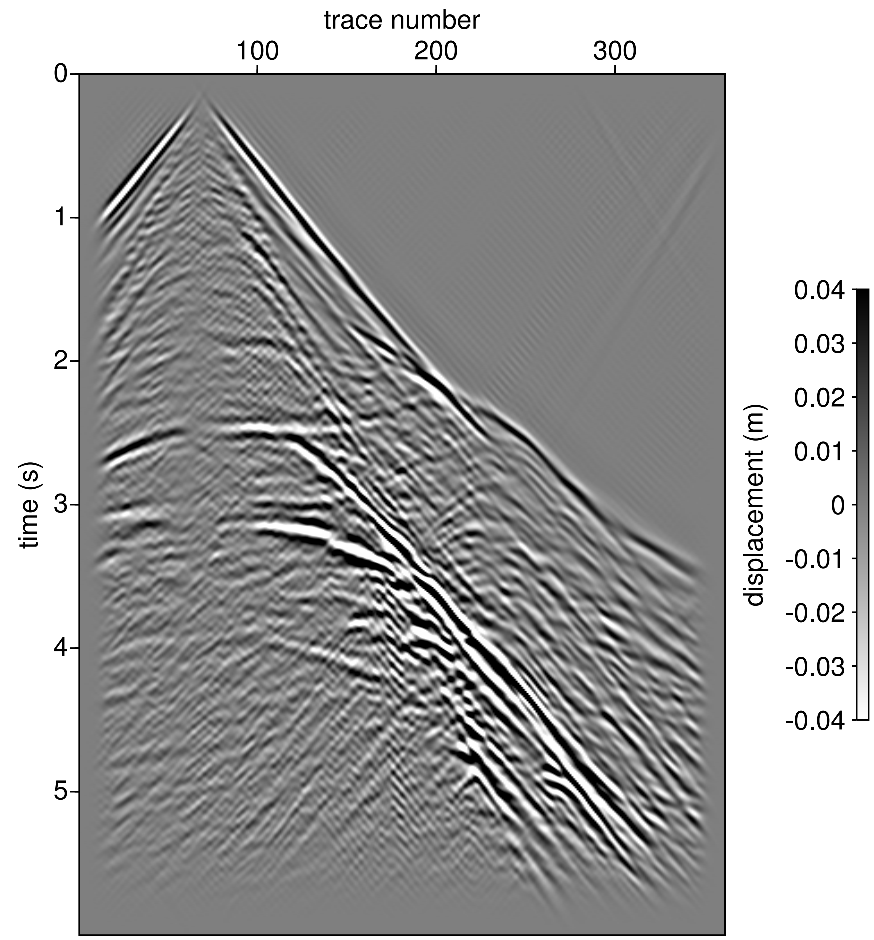

final processed data (shot 20, X-comp)

A realistic synthetic model: multiscale data

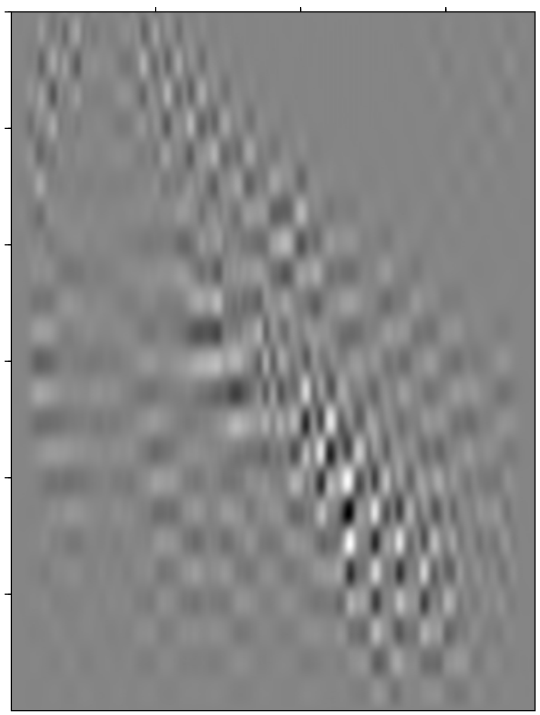

D12 scale 9

A realistic synthetic model: multiscale data

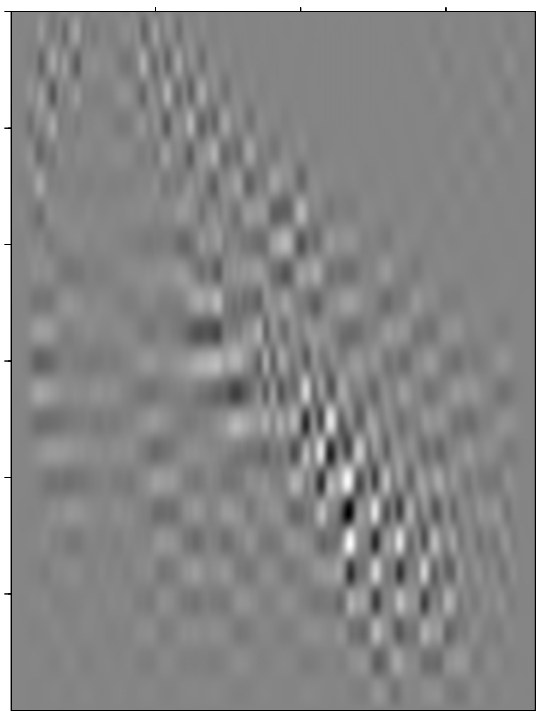

D12 scale 9

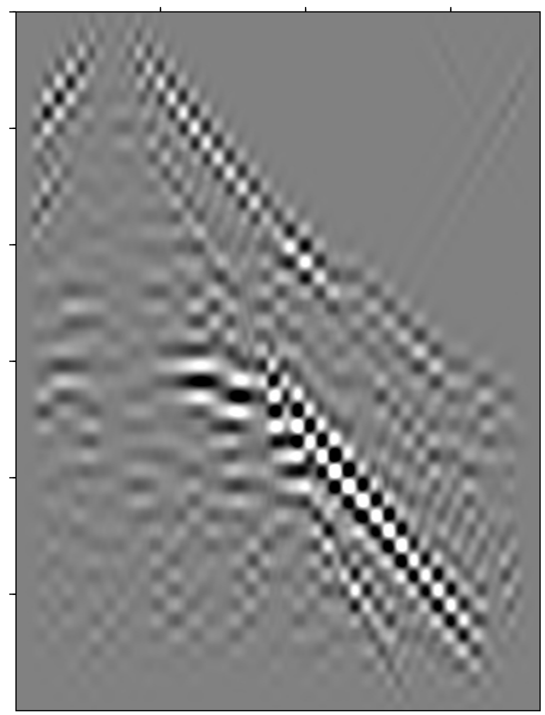

D12 scale 8

A realistic synthetic model: multiscale data

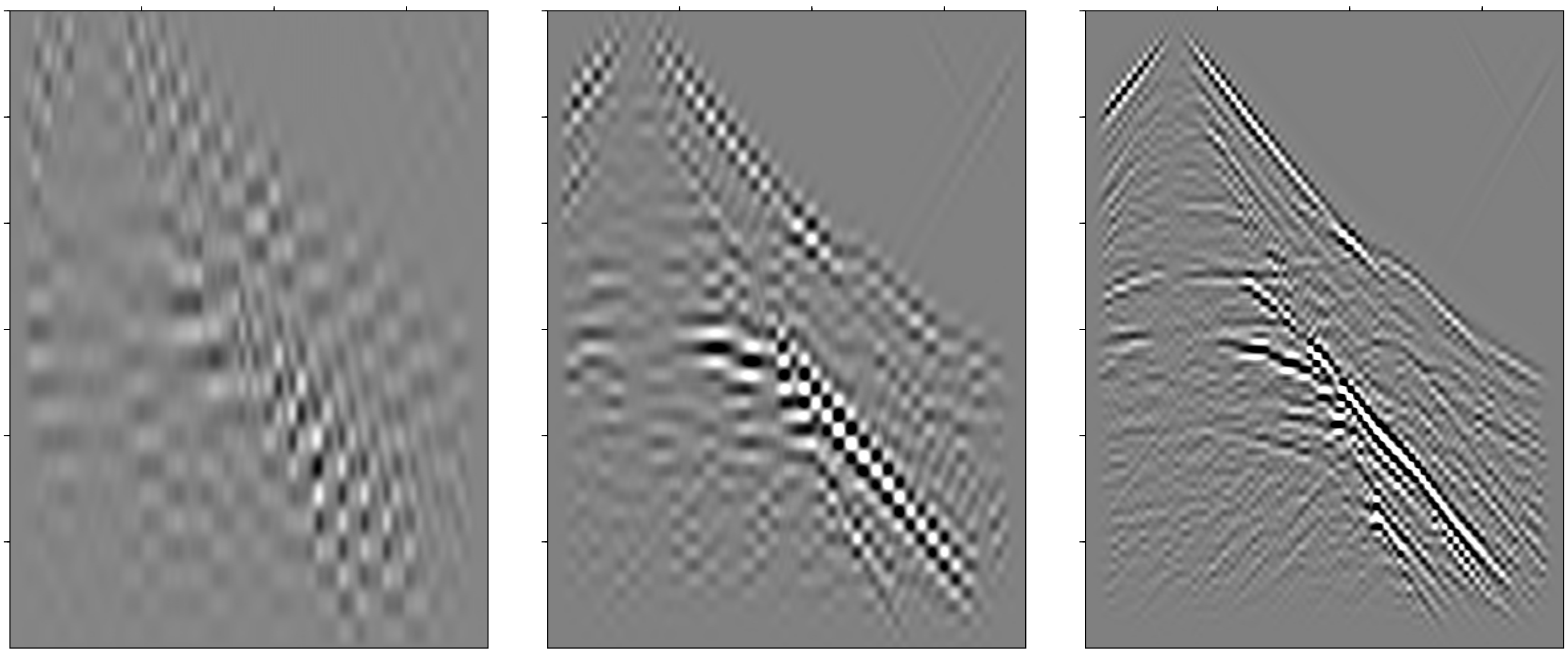

D12 scale 9 D12 scale 8 D12 scale 7

Misfit gradient: Initial model, full resolution

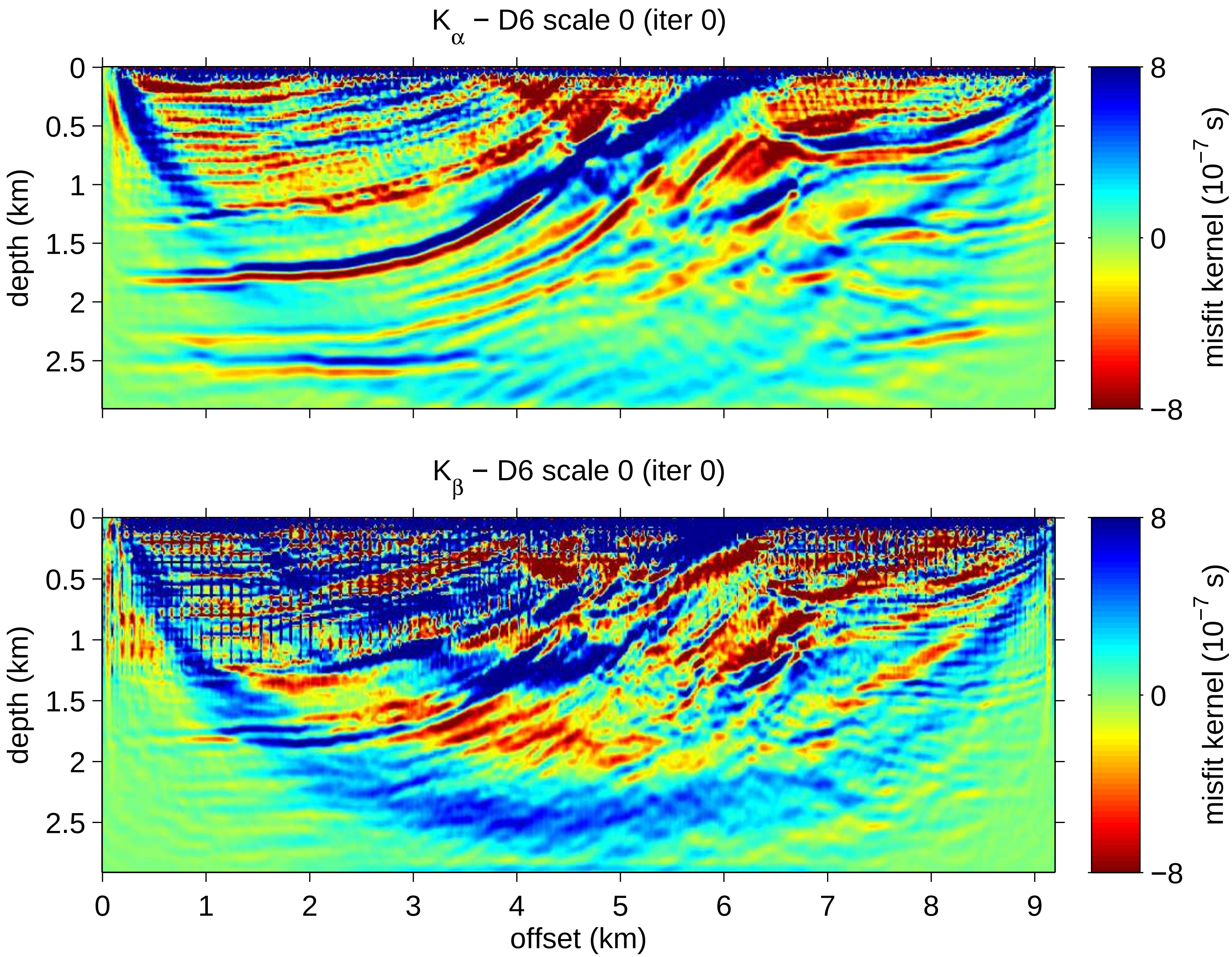

Yuan & Simons, *Geophysics* (2014)

Misfit gradient: Initial model, data at scale 9

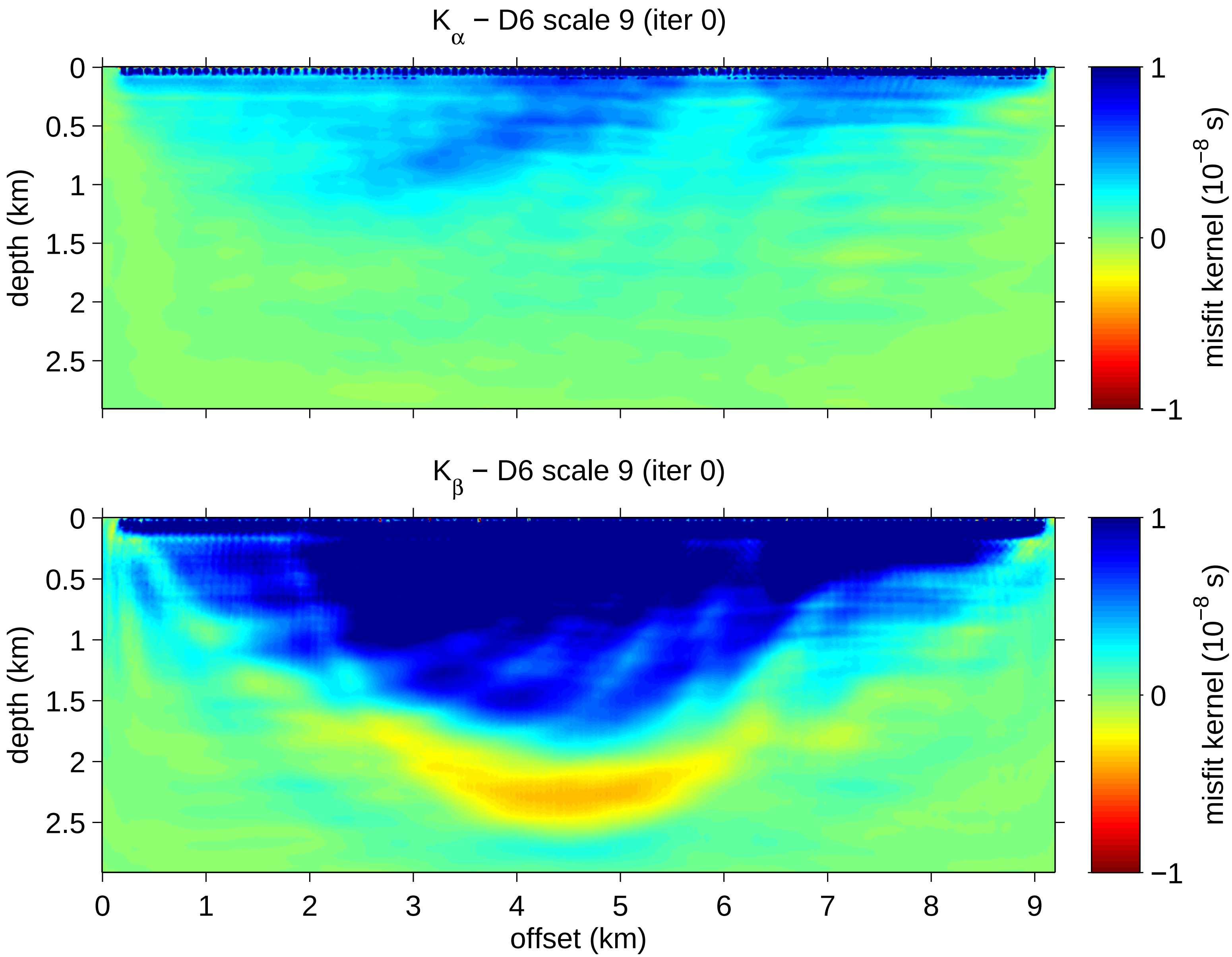

Yuan & Simons, *Geophysics* (2014)

Misfit gradient: 4 iterations, data at scale 9

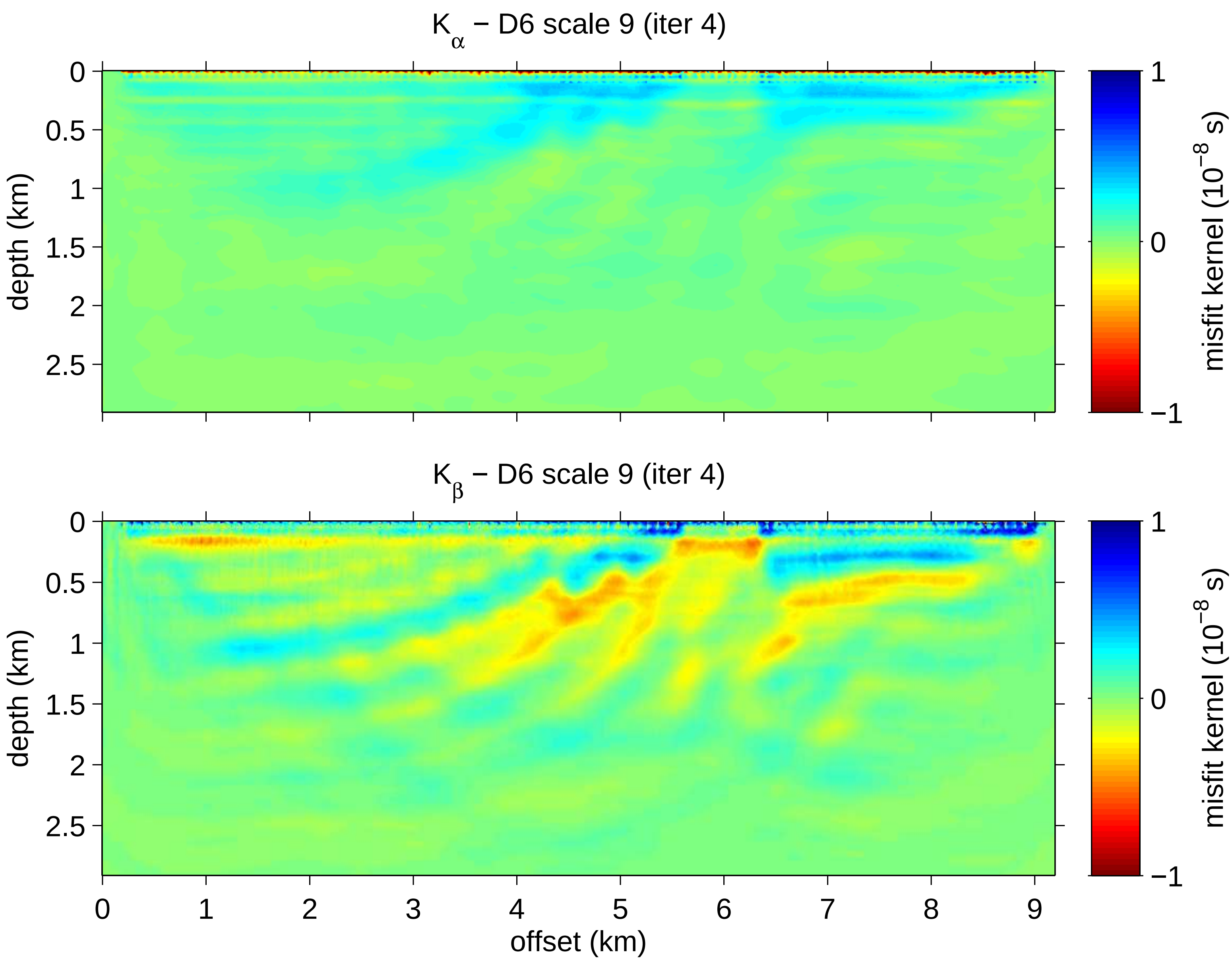

Misfit gradient: 4 iterations, data at scale 8

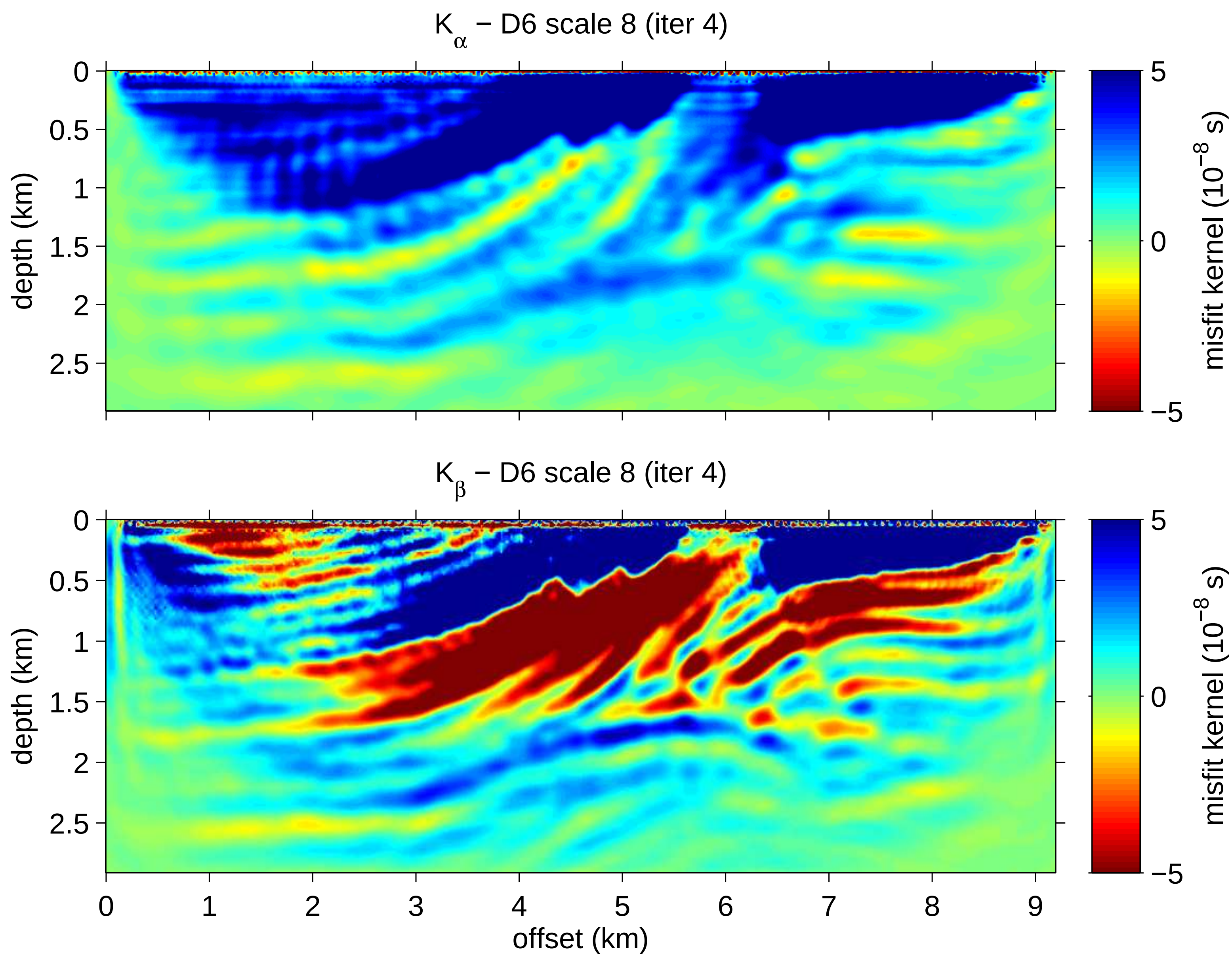

Yuan & Simons, *Geophysics* (2014)

Misfit gradient: 31 iterations, data at scale 8

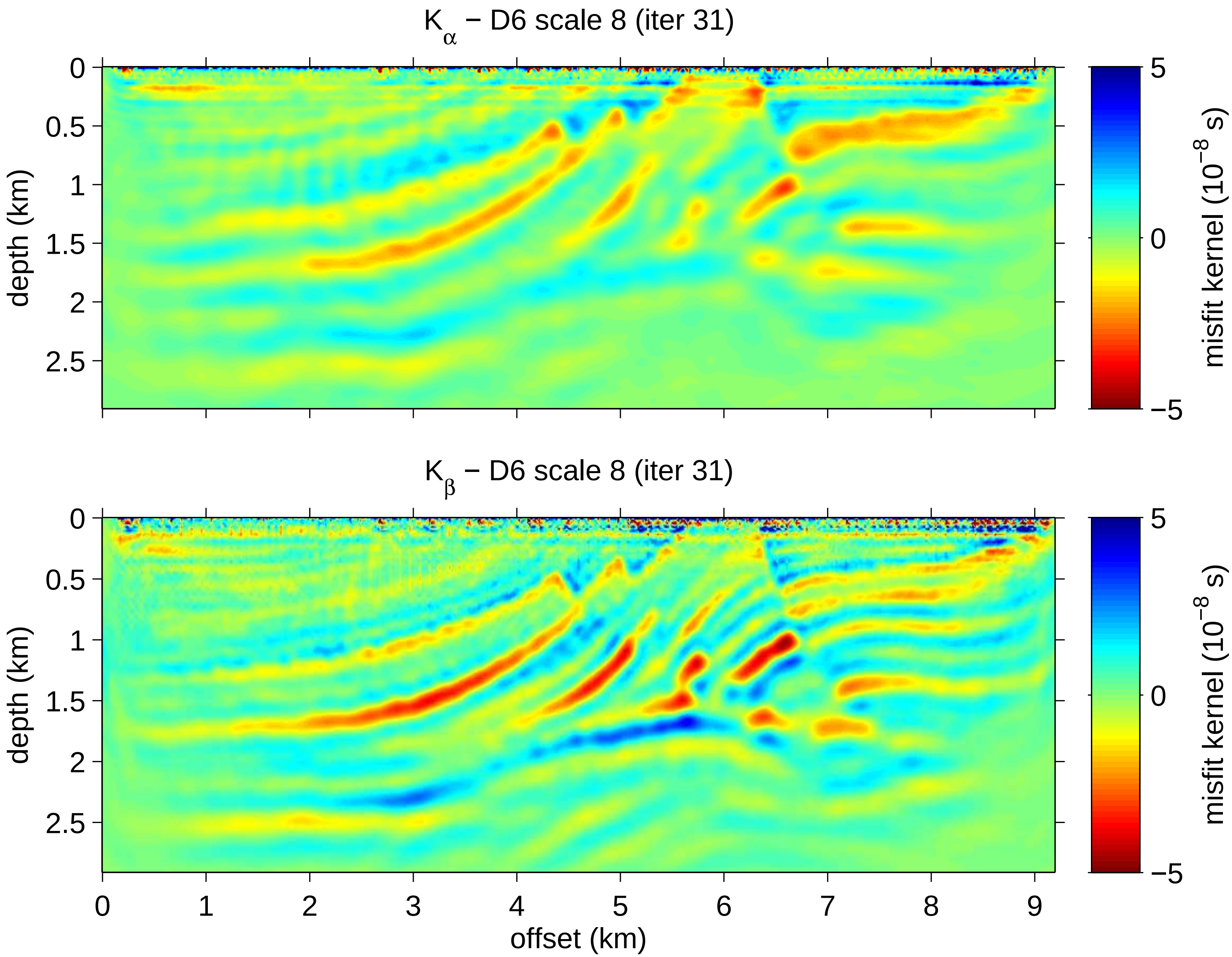

Yuan & Simons, *Geophysics* (2014)

Iteration path

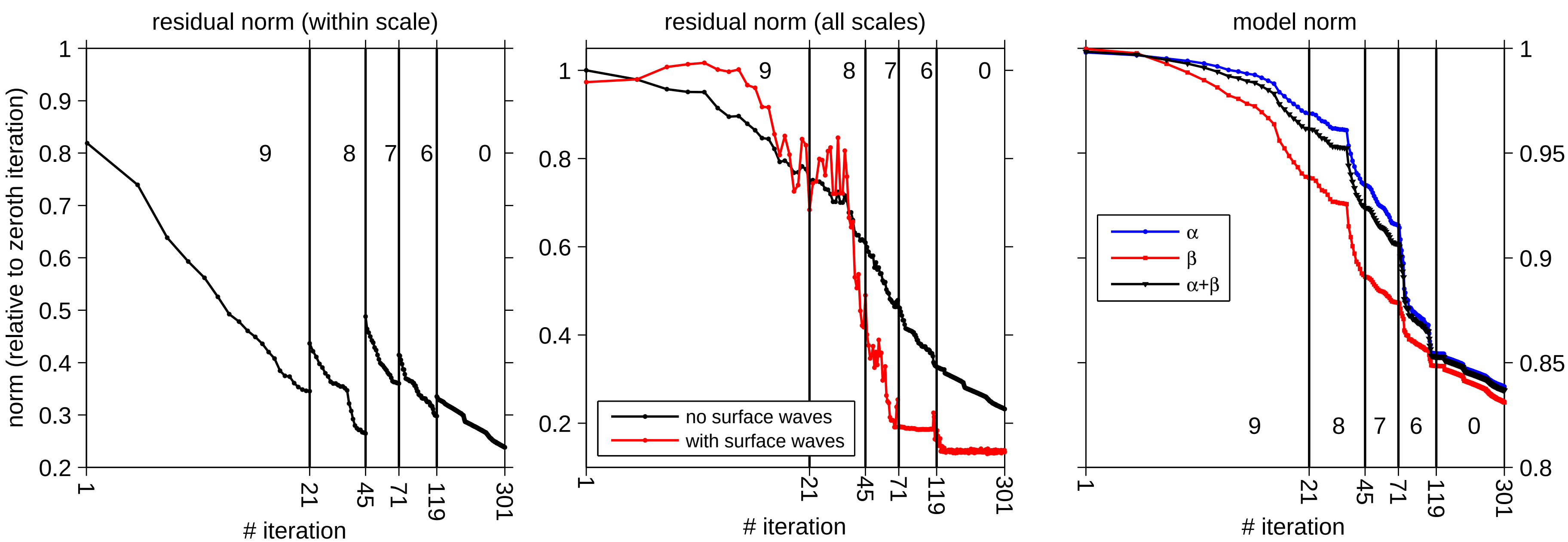

Final model

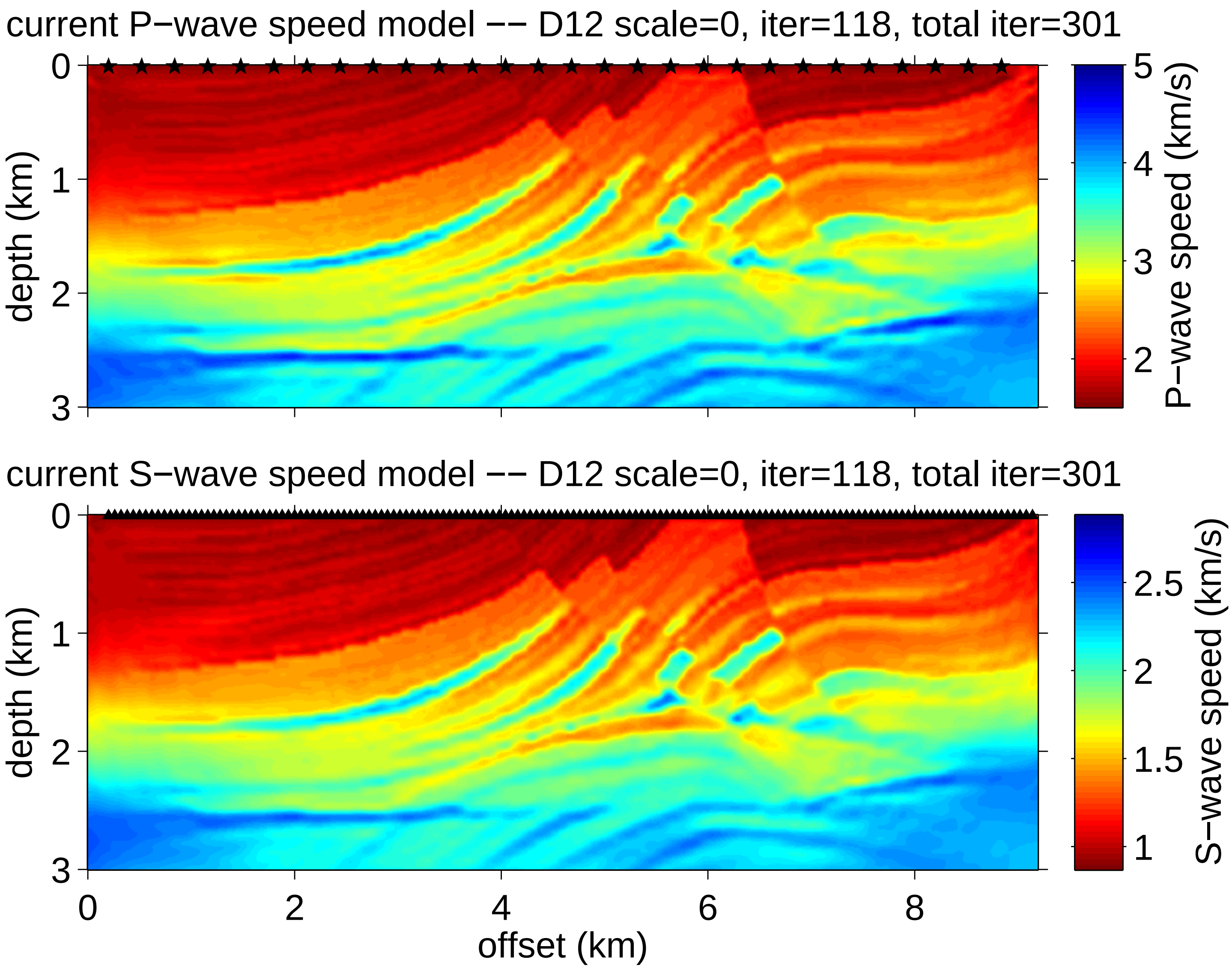

Yuan & Simons, *Geophysics* (2014)

Target & Initial models

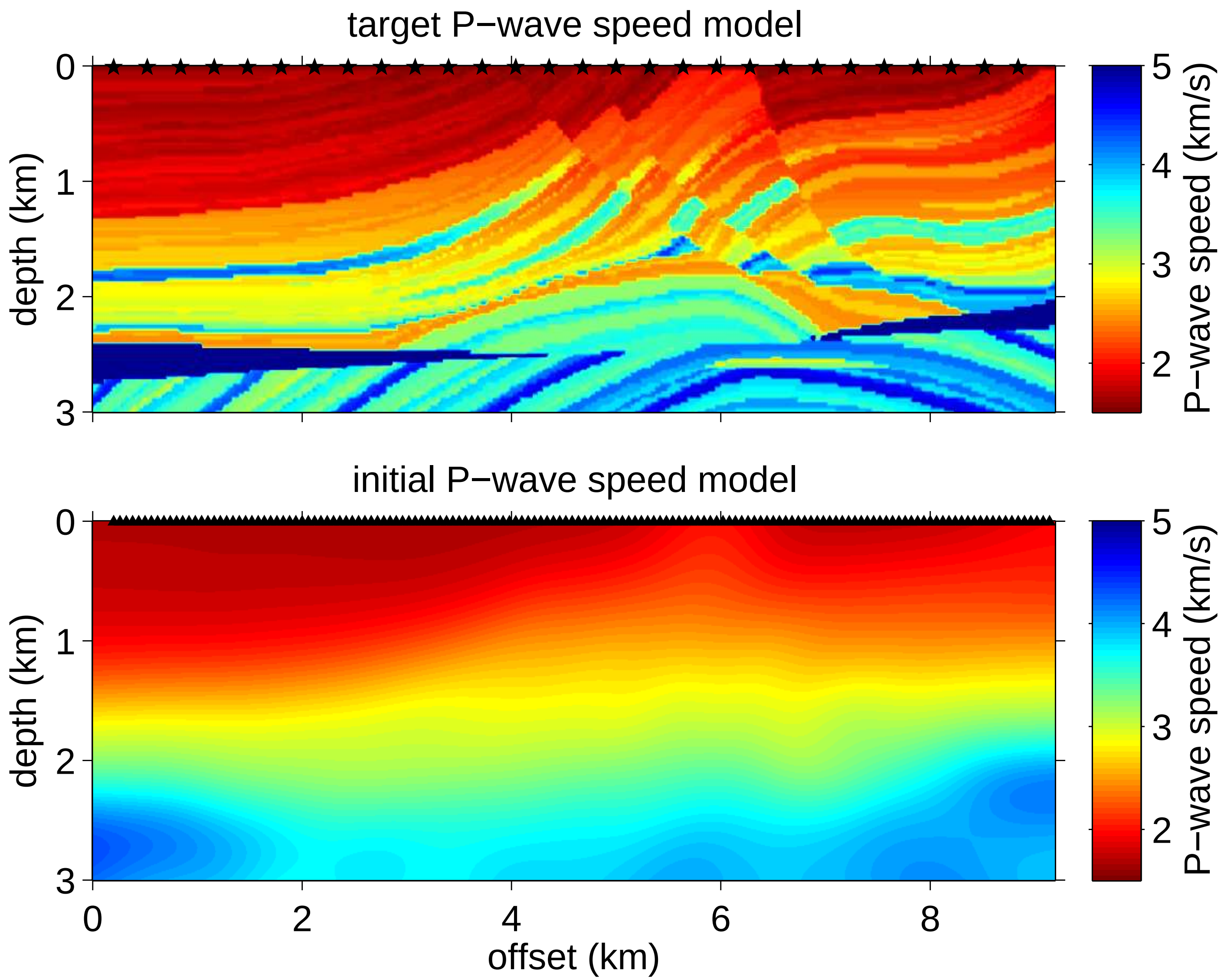

Yuan & Simons, *Geophysics* (2014)

Conclusions — I

1. Rather than reparameterizing the model, or enforcing sparsity, we use a **wavelet multiscale decomposition** of the seismogram to precondition the inverson.

Conclusions — I

1. Rather than reparameterizing the model, or enforcing sparsity, we use a **wavelet multiscale decomposition** of the seismogram to precondition the inverson.

2. The **data** are wavelet transformed before subjecting to an **elastic full-waveform inversion** using an **adjoint** formalism. Surface waves are removed.

Conclusions — I

1. Rather than reparameterizing the model, or enforcing sparsity, we use a **wavelet multiscale decomposition** of the seismogram to precondition the inverson.

2. The **data** are wavelet transformed before subjecting to an **elastic full-waveform inversion** using an **adjoint** formalism. Surface waves are removed.

3. The misfit function is the **mean-squared error** over the observation window.

Conclusions — I

1. Rather than reparameterizing the model, or enforcing sparsity, we use a **wavelet multiscale decomposition** of the seismogram to precondition the inverson.

2. The **data** are wavelet transformed before subjecting to an **elastic full-waveform inversion** using an **adjoint** formalism. Surface waves are removed.

3. The misfit function is the **mean-squared error** over the observation window.

4. Successively more detailed wavelet-reconstructed seismograms are fed to the algorithm in a way that successfully **conditions the misfit function** to obtain excellent final fits at low computational costs.

Conclusions — I

1. Rather than reparameterizing the model, or enforcing sparsity, we use a **wavelet multiscale decomposition** of the seismogram to precondition the inverson.
2. The **data** are wavelet transformed before subjecting to an **elastic full-waveform inversion** using an **adjoint** formalism. Surface waves are removed.
3. The misfit function is the **mean-squared error** over the observation window.
4. Successively more detailed wavelet-reconstructed seismograms are fed to the algorithm in a way that successfully **conditions the misfit function** to obtain excellent final fits at low computational costs.
5. **Complicated target models** can be fit starting from even **poor initial models**.

Waveform *envelope-difference*

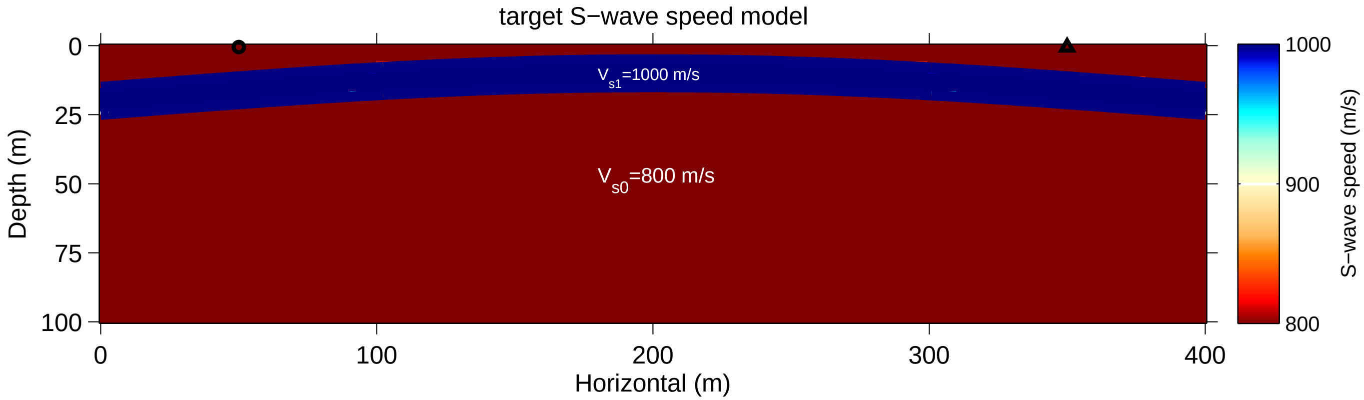

Waveform *envelope-difference*

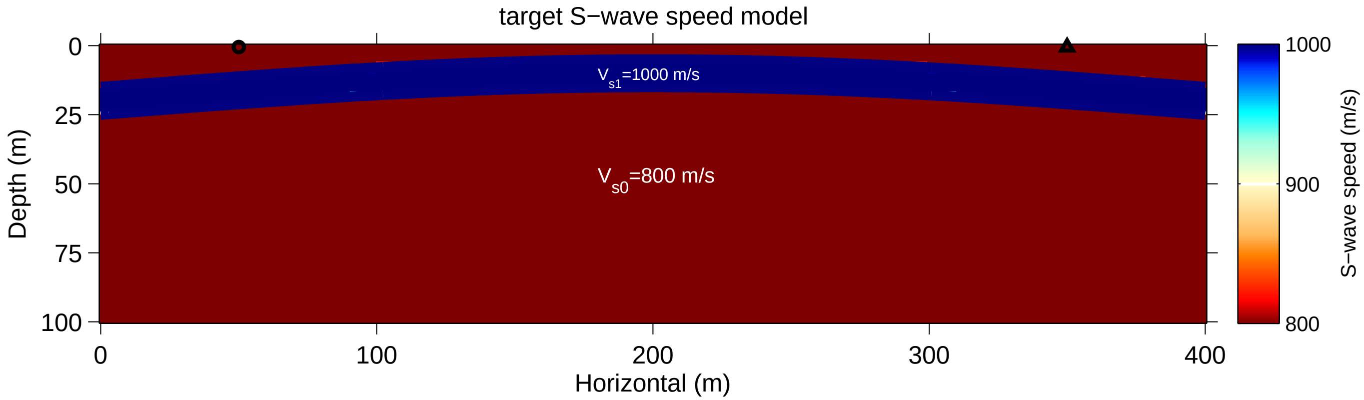

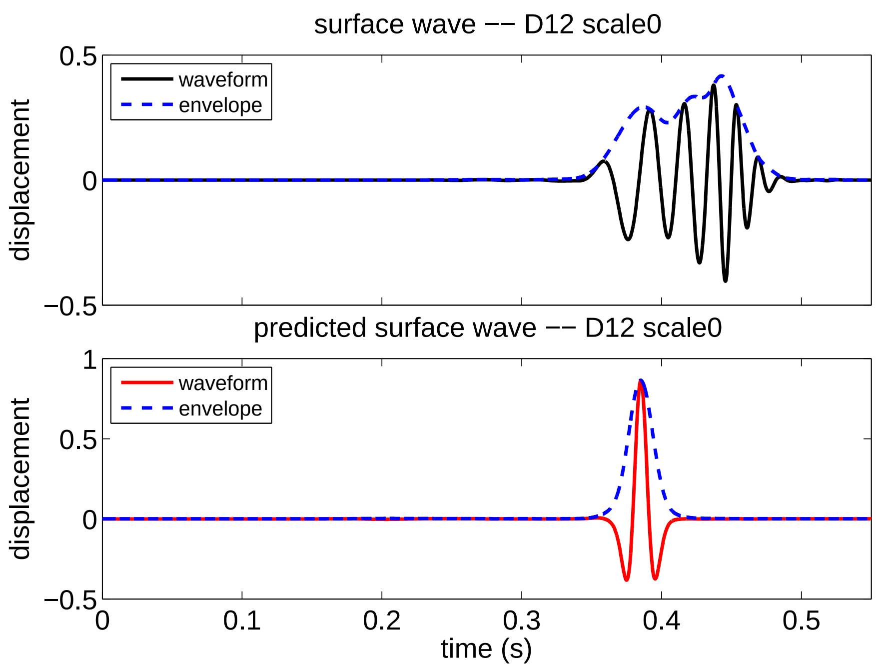

Waveform *envelope-difference*

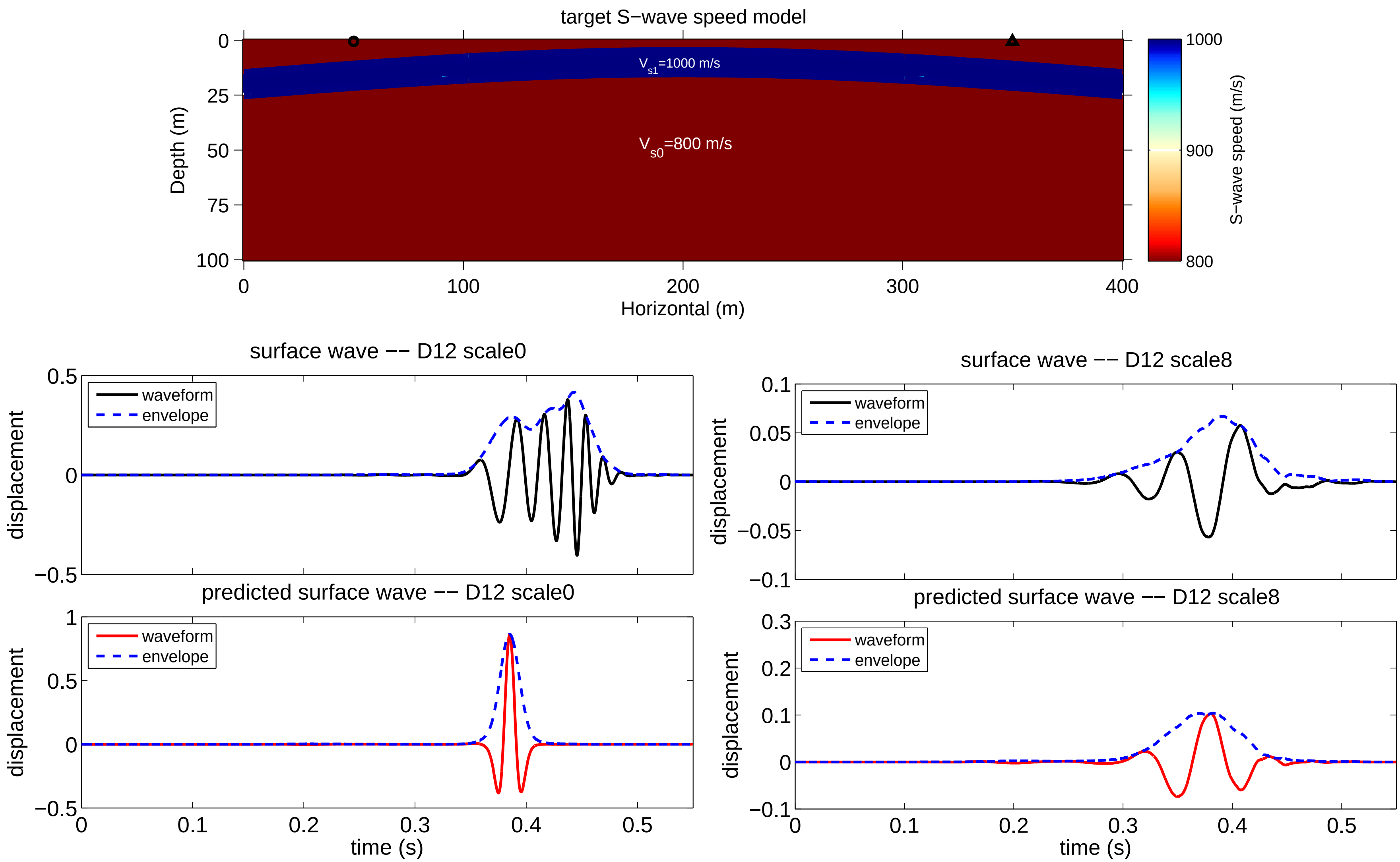

Yuan & Simons, *in preparation* (2015)

Multiscale adjoint waveform-*envelope-difference*

1. Misfit for model $\mathbf{m}$, envelope E, data/synthetic component d, s, at $\mathbf{x}$ & t:
$\chi(\mathbf{m}) = \frac{1}{2}\sum_{s,r}\int_0^T ||E^s(\mathbf{x}_r, \mathbf{x}_s, t; \mathbf{m}) - E^d(\mathbf{x}_r, \mathbf{x}_s, t)||^2 \, dt.$

Multiscale adjoint waveform-*envelope-difference*

1. Misfit for model $\mathbf{m}$, envelope E, data/synthetic component d, s, at $\mathbf{x}$ & t:
   $\chi(\mathbf{m}) = \frac{1}{2}\sum_{s,r}\int_0^T ||E^s(\mathbf{x}_r, \mathbf{x}_s, t; \mathbf{m}) - E^d(\mathbf{x}_r, \mathbf{x}_s, t)||^2 \, dt.$
2. Derivative of $\chi(\mathbf{m})$ over sources/receivers s, r, with Hilbert transform $\mathcal{H}$:
   $\delta\chi(\mathbf{m}) = \sum_{s,r}\int_0^T \left[E_1^{ratio}\ s - \mathcal{H}\{E_1^{ratio}\ (\mathcal{H}s)\}\right] \delta s \, dt$

Multiscale adjoint waveform-*envelope-difference*

1. Misfit for model $\mathbf{m}$, envelope E, data/synthetic component d, s, at $\mathbf{x}$ & t:
   $\chi(\mathbf{m}) = \frac{1}{2} \sum_{s,r} \int_0^T ||E^s(\mathbf{x}_r, \mathbf{x}_s, t; \mathbf{m}) - E^d(\mathbf{x}_r, \mathbf{x}_s, t)||^2 \, dt.$
2. Derivative of $\chi(\mathbf{m})$ over sources/receivers s, r, with Hilbert transform $\mathcal{H}$:
   $\delta\chi(\mathbf{m}) = \sum_{s,r} \int_0^T \left[E_1^{ratio} \; s - \mathcal{H}\{E_1^{ratio} \; (\mathcal{H}s)\}\right] \delta s \, dt$
3. Linearized expression under the Born approximation

Multiscale adjoint waveform-*envelope-difference*

1. Misfit for model $\mathbf{m}$, envelope E, data/synthetic component d, s, at $\mathbf{x}$ & t:
   $\chi(\mathbf{m}) = \frac{1}{2} \sum_{s,r} \int_0^T ||E^s(\mathbf{x}_r, \mathbf{x}_s, t; \mathbf{m}) - E^d(\mathbf{x}_r, \mathbf{x}_s, t)||^2 \, dt.$
2. Derivative of $\chi(\mathbf{m})$ over sources/receivers s, r, with Hilbert transform $\mathcal{H}$:
   $\delta\chi(\mathbf{m}) = \sum_{s,r} \int_0^T \left[E_1^{ratio} \; s - \mathcal{H}\{E_1^{ratio} \; (\mathcal{H}s)\}\right] \delta s \, dt$
3. Linearized expression under the Born approximation

4. Misfit kernel

Multiscale adjoint waveform-*envelope-difference*

1. Misfit for model $\mathbf{m}$, envelope E, data/synthetic component d, s, at $\mathbf{x}$ & t:
   $\chi(\mathbf{m}) = \frac{1}{2} \sum_{s,r} \int_0^T ||E^s(\mathbf{x}_r, \mathbf{x}_s, t; \mathbf{m}) - E^d(\mathbf{x}_r, \mathbf{x}_s, t)||^2 \, dt.$
2. Derivative of $\chi(\mathbf{m})$ over sources/receivers s, r, with Hilbert transform $\mathcal{H}$:
   $\delta\chi(\mathbf{m}) = \sum_{s,r} \int_0^T \left[E_1^{ratio} \; s - \mathcal{H}\{E_1^{ratio} \; (\mathcal{H}s)\}\right] \delta s \, dt$
3. Linearized expression under the Born approximation
4. Misfit kernel
5. The new **adjoint** field $\mathrm{s}^\dagger$ appropriate for this new observation.

Multiscale adjoint waveform-*envelope-difference*

1. Misfit for model $\mathbf{m}$, envelope E, data/synthetic component d, s, at $\mathbf{x}$ & t:
   $\chi(\mathbf{m}) = \frac{1}{2}\sum_{s,r}\int_0^T ||E^s(\mathbf{x}_r, \mathbf{x}_s, t; \mathbf{m}) - E^d(\mathbf{x}_r, \mathbf{x}_s, t)||^2 \, dt.$
2. Derivative of $\chi(\mathbf{m})$ over sources/receivers s, r, with Hilbert transform $\mathcal{H}$:
   $\delta\chi(\mathbf{m}) = \sum_{s,r}\int_0^T \left[E_1^{ratio} \; s - \mathcal{H}\{E_1^{ratio} \; (\mathcal{H}s)\}\right] \delta s \, dt$
3. Linearized expression under the Born approximation
4. Misfit kernel
5. The new **adjoint** field $\mathrm{s}^\dagger$ appropriate for this new observation.
6. Our innovation is to switch from multiscale (1) surface-wave *envelope*-difference to (2) surface-wave *waveform*-difference to (3) surface- and body-wave *waveform*-difference adjoint inversions.

A realistic synthetic model

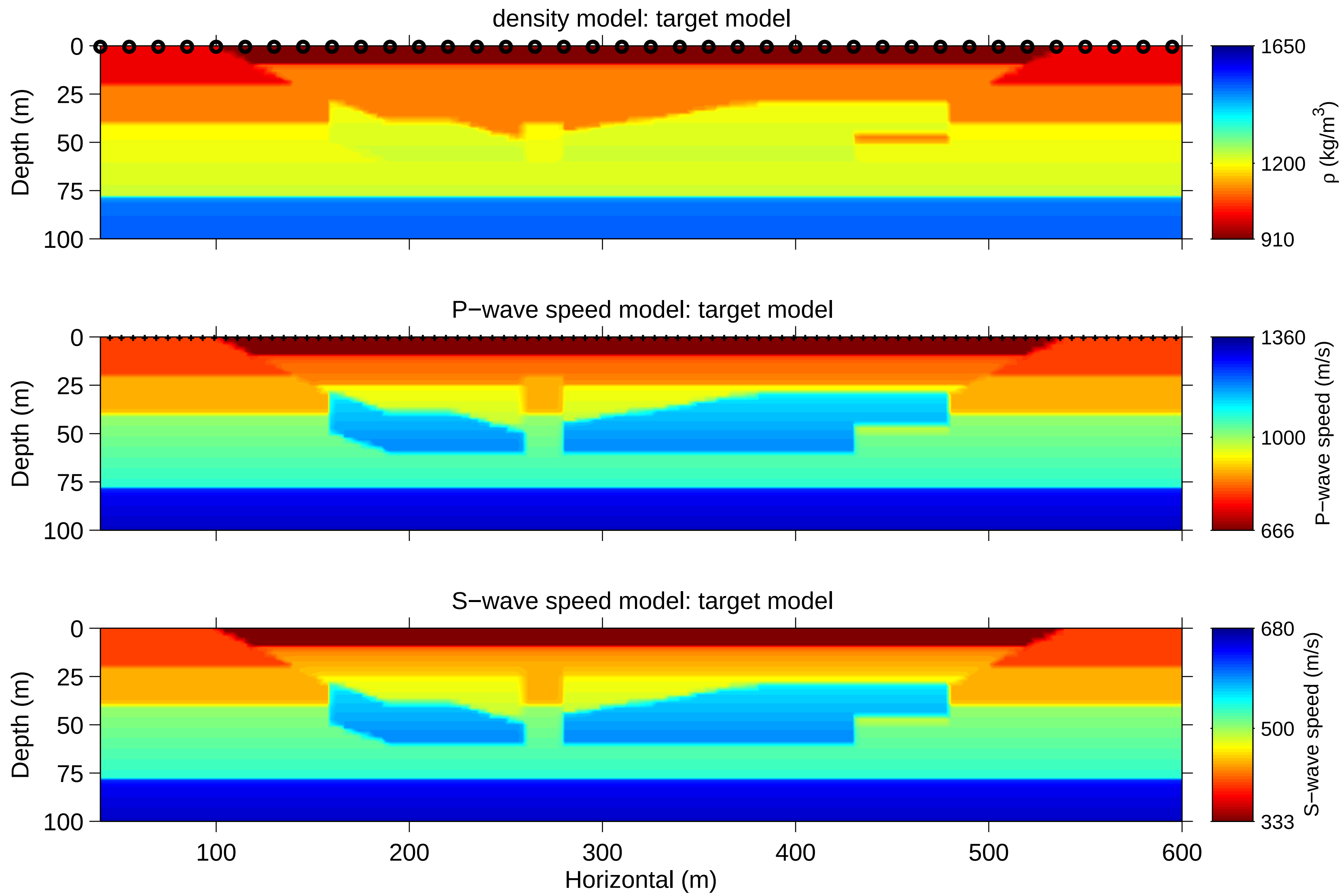

Yuan, Simons & Bozdağ, *in preparation* (2015)

“Final” model — Surface waves only

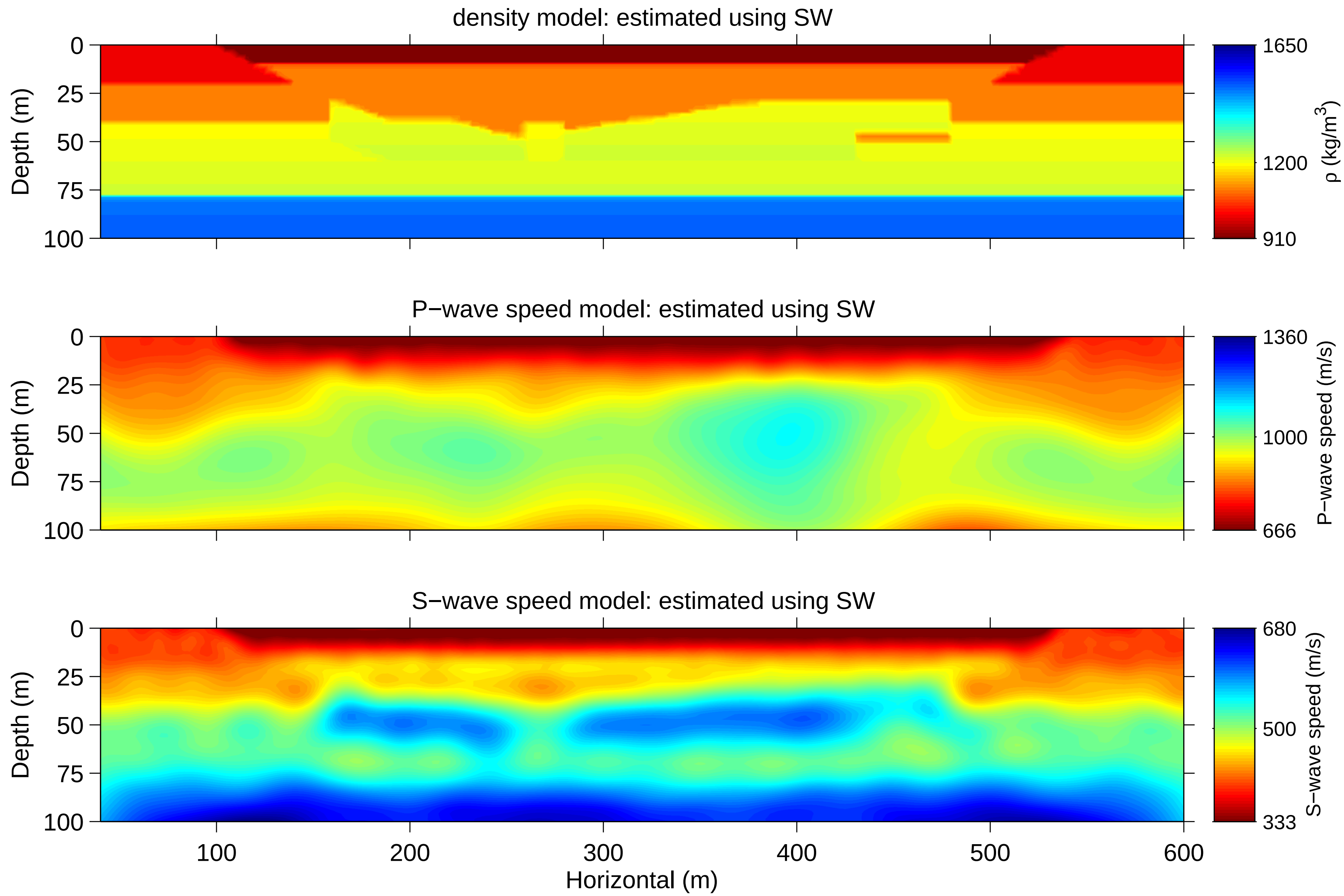

Yuan, Simons & Bozdağ, *in preparation* (2015)

"Final" model — Body waves only

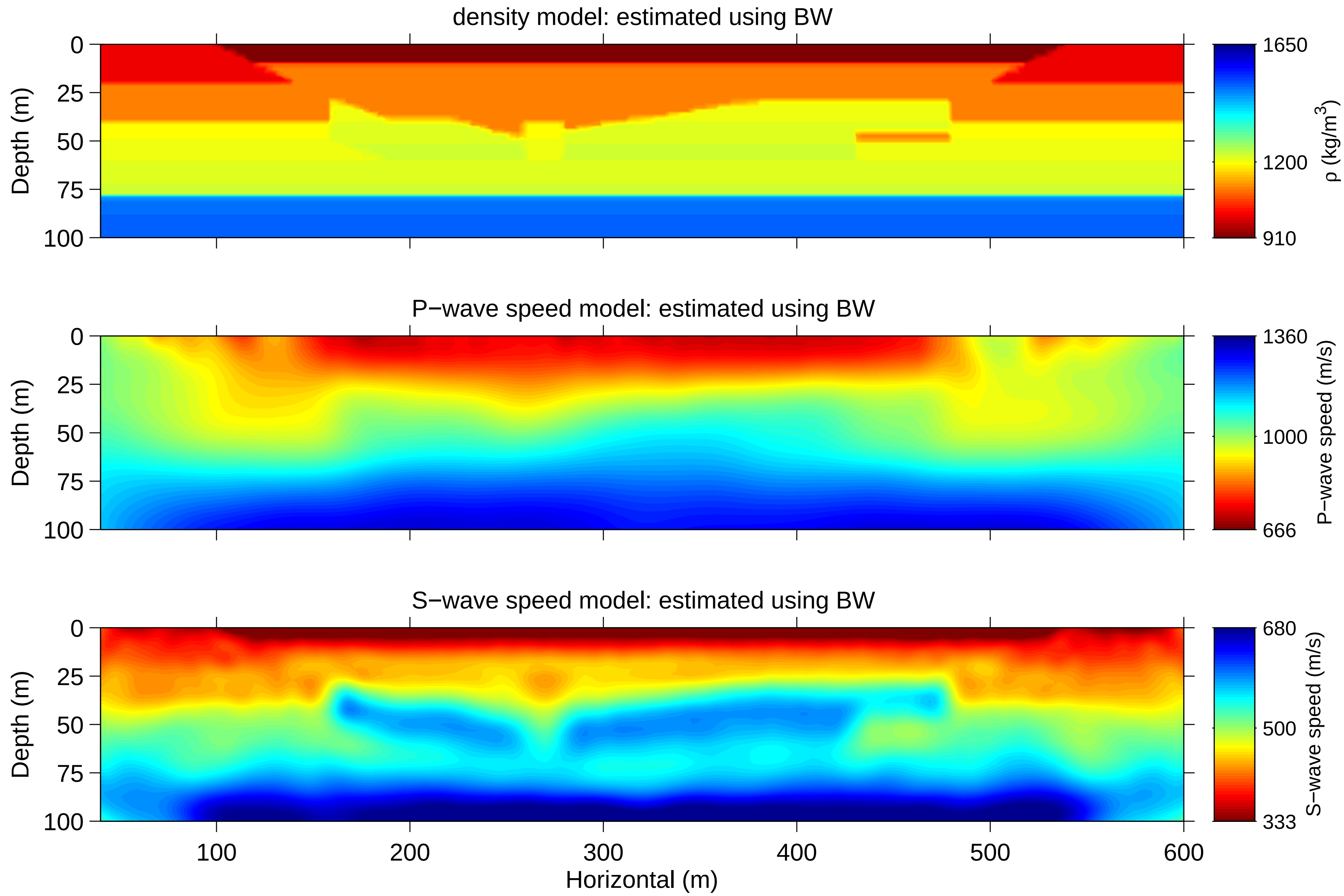

Yuan, Simons & Bozdağ, *in preparation* (2015)

Final model — Body and surface waves

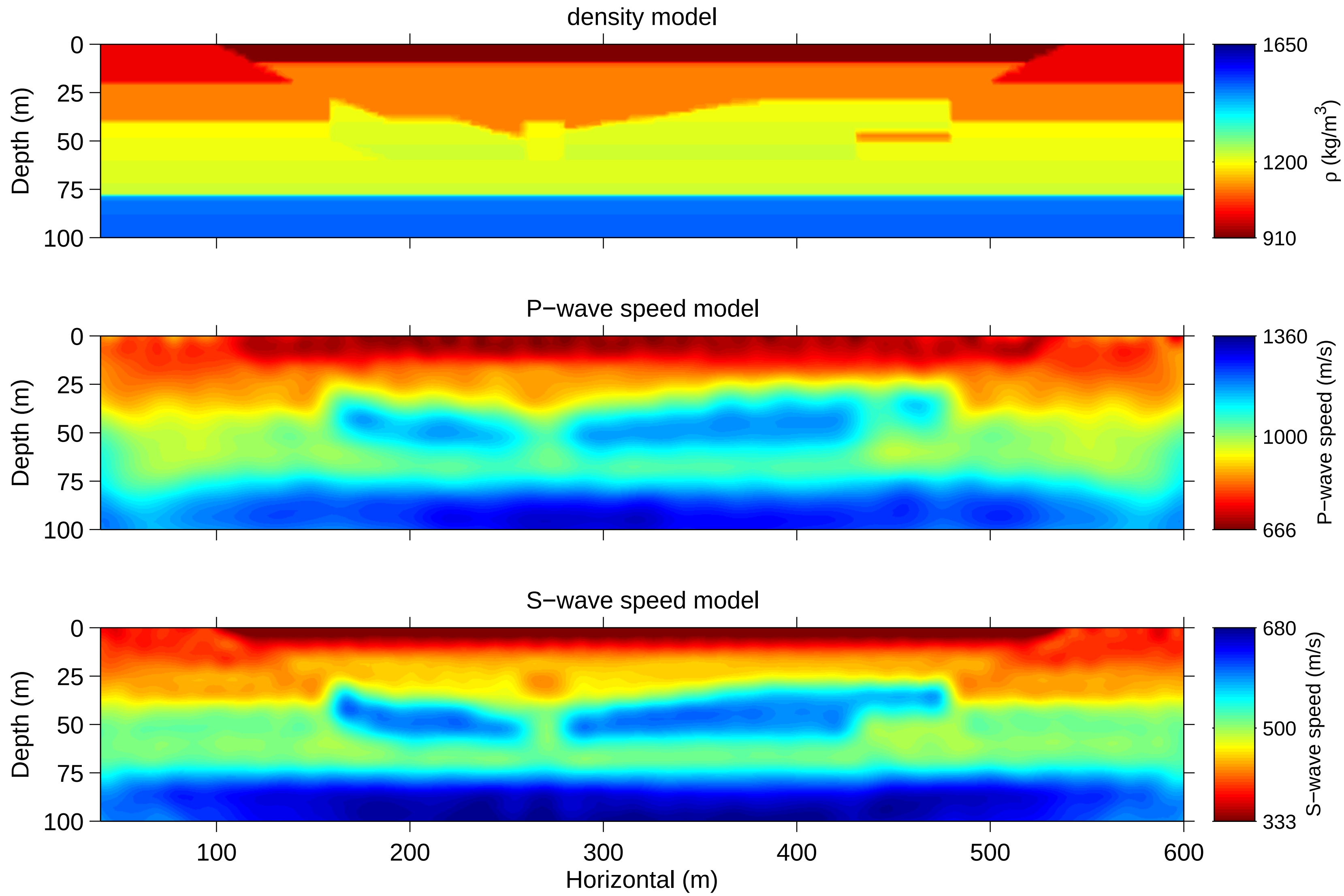

Target model

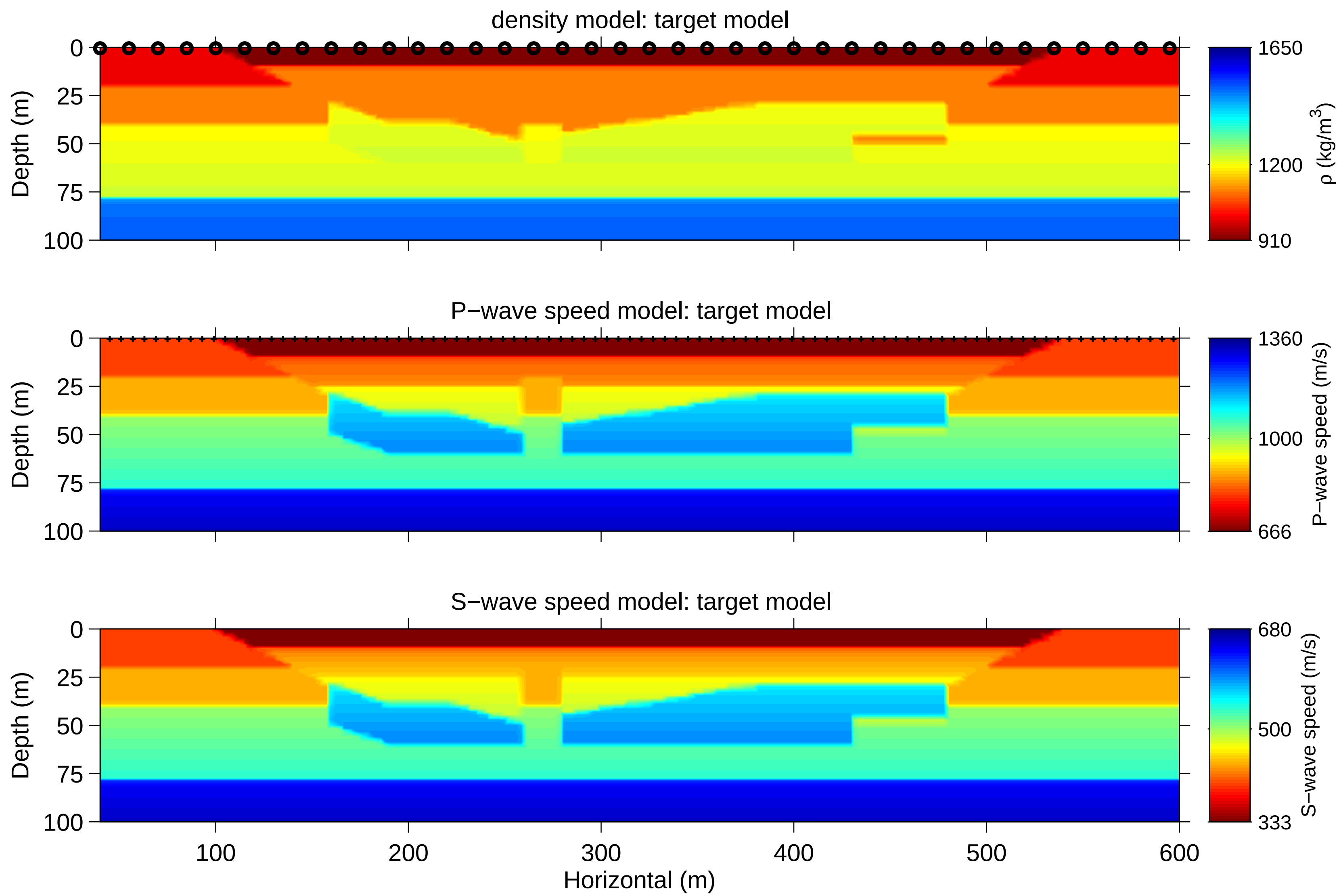

Yuan, Simons & Bozdağ, *in preparation* (2015)

Conclusions — II

1. **Multiresolution wavelet decompositions of the seismograms** prior to measurement successfully coax the full-waveform inverse adjoint problem into well-behaved territory

Conclusions — II

1. **Multiresolution wavelet decompositions of the seismograms** prior to measurement successfully coax the full-waveform inverse adjoint problem into well-behaved territory

2. **Surface waves** are important, and not only for the shallowmost structure

Conclusions — II

1. **Multiresolution wavelet decompositions of the seismograms** prior to measurement successfully coax the full-waveform inverse adjoint problem into well-behaved territory

2. **Surface waves** are important, and not only for the shallowmost structure

3. Generally considered a nuisance, they can be **fully embraced**

Conclusions — II

1. **Multiresolution wavelet decompositions of the seismograms** prior to measurement successfully coax the full-waveform inverse adjoint problem into well-behaved territory

2. **Surface waves** are important, and not only for the shallowmost structure

3. Generally considered a nuisance, they can be **fully embraced**

4. For *surface* waves, we measure multiscale **waveform envelope differences**

Conclusions — II

1. **Multiresolution wavelet decompositions of the seismograms** prior to measurement successfully coax the full-waveform inverse adjoint problem into well-behaved territory

2. **Surface waves** are important, and not only for the shallowmost structure

3. Generally considered a nuisance, they can be **fully embraced**

4. For *surface* waves, we measure multiscale **waveform envelope differences**

5. For *body* waves, we measure multiscale **waveform differences**

Conclusions — II

1. **Multiresolution wavelet decompositions of the seismograms** prior to measurement successfully coax the full-waveform inverse adjoint problem into well-behaved territory

2. **Surface waves** are important, and not only for the shallowmost structure

3. Generally considered a nuisance, they can be **fully embraced**

4. For *surface* waves, we measure multiscale **waveform envelope differences**

5. For *body* waves, we measure multiscale **waveform differences**

6. Our algorithm switches from (1) surface-wave ED to (2) surface-wave WD to (3) complete-seismogram WD, descending down the wavelet scales from coarse to full resolution until convergence